

Proposal for an optical interferometric measurement of the gravitational redshift with satellite systems

Daniel R. Terno^{1,*} Francesco Vedovato^{2,3} Matteo Schiavon^{2,3,4} Alexander R. H. Smith,^{5,6}
Piergiovanni Magnani,⁷ Giuseppe Vallone^{2,3,8} and Paolo Villorresi^{2,3,†}

¹*School of Mathematical and Physical Sciences, Macquarie University,
Sydney, New South Wales 2109, Australia*

²*Dipartimento di Ingegneria dell'Informazione, Università degli Studi di Padova, Padova 35131, Italy*

³*Istituto Nazionale di Fisica Nucleare (INFN)—Sezione di Padova, Via Marzolo 8, Padova 35131, Italy*


⁴*Sorbonne Université, CNRS, LIP6, F-75005 Paris, France*

⁵*Department of Physics, Saint Anselm College, Manchester, New Hampshire 03102, USA*

⁶*Department of Physics and Astronomy, Dartmouth College, Hanover, New Hampshire 03755, USA*

⁷*Department of Physics, Politecnico di Milano, Milano 20133, Italy*

⁸*Dipartimento di Fisica e Astronomia, Università di Padova, via Marzolo 8, 35131 Padova, Italy*

 (Received 13 February 2023; accepted 14 September 2023; published 30 October 2023)

The Einstein equivalence principle (EEP) underpins all metric theories of gravity. One of its key aspects is the local position invariance of nongravitational experiments, which is captured by the gravitational redshift. The iconic gravitational redshift experiment places two fermionic systems, used as clocks, in different gravitational potentials and compares them using the electromagnetic field. However, the electromagnetic field itself can be used as a clock, by comparing the phases acquired by two optical pulses propagating through different gravitational potentials. A fundamental point in the implementation of a space-based large-distance optical interferometric experiment is the suppression of the first-order Doppler effect, which dominates the weak gravitational signal necessary to test the EEP. Here, we propose a novel scheme to suppress it by subtracting the phase-shifts measured in a one-way and two-way configuration between a ground station and a satellite. We present a detailed analysis of this technique within the post-Newtonian framework and perform simulations of its performance using realistic satellite orbits and state-of-the-art fiber technology at the telecom wavelength of 1550 nm.

DOI: [10.1103/PhysRevD.108.084063](https://doi.org/10.1103/PhysRevD.108.084063)

I. INTRODUCTION

Light, apart from the *ad hoc* applications of corpuscular analogies, is insensitive to Newtonian gravity. The situation is conceptually very different in general relativity (GR): in all metric theories of gravity, electromagnetic (EM) wave propagation depends on the spacetime background [1–3]. In the short wavelength limit, light rays [4], which are characteristic curves of the wave equation, model classical and quantum beams, as well as trajectories of single photons [4–6]. On curved backgrounds, the short-wave asymptotic expansion identifies rays as null geodesics [1,3]. However, near the surface of our planet the gravitational effects appear at the c^{-2} post-Newtonian order, where c is the speed of light. Much stronger kinematic effects often mask these second-order terms.

For example, the optical version of the Colella-Overhauser-Werner (COW) experiment [7] was proposed

in [8]. Using communication between a spacecraft and a ground station to realize the Mach-Zehnder interferometer (the experiment was suggested in [9] as a possible component of the QEYSSAT mission [10]), it is possible to obtain a large gravitationally induced phase shift,

$$\varphi_{\text{gr}} = \Delta U \omega_0 \tau_l \approx -\frac{gh}{c^2} \frac{2\pi}{\lambda} nl. \quad (1)$$

In this scheme a photon time-bin superposition [11] is sent from a ground station on Earth to a spacecraft. Both terminals are equipped with a fiber-based interferometer of equal temporal imbalance $\tau_l = nl/c$ (with $n = 1.5$ the refractive index of the fiber and l the length of the delay line), to temporally recombine the two time bins and obtain an interference pattern depending on the gravitational phase-shift $\varphi_{\text{gr}} = \Delta\omega\tau_l$ [12], where the frequency shift $\Delta\omega$ is derived in Eq. (2). Here we approximated the difference of the dimensionless gravitational potential as $-gh/c^2$, with g the Earth's gravity and h the satellite altitude, and $\lambda = 2\pi c/\omega_0$ is the sent wavelength. The order of magnitude of the gravitational redshift is about 1 rad, supposing $\lambda = 1550$ nm,

* daniel.terno@mq.edu.au

† paolo.villorresi@dei.unipd.it

$l = 1.2$ km, and an altitude $h = 1500$ km (which corresponds to $\Delta U \approx -1.3 \times 10^{-10}$ [13]). The expected signal lies in a measurable regime, and an optical precision of $\delta\varphi_{\text{gr}} \approx 10 \mu\text{rad}$ is experimentally achievable provided a number of detected photons N fulfilling $N \gtrsim 1/\delta\varphi_{\text{gr}}^2$ [14].

However, a careful analysis of the optical COW experiment in [15] showed that the first-order Doppler effect is roughly 10^5 times stronger than the desired signal φ_{gr} . Moreover, in this setting the kinematic and gravitational effects are ineludibly linked [12]. This first-order Doppler effect was recently measured by exploiting large-distance precision interferometry along space channels [16], which represents a resource for performing fundamental tests of quantum mechanics in space, as in [8,17–20], for future space-based scientific missions, such as LISA [21], and space-based quantum cryptography [22–27].

A novel proposal for the extraction of the gravitational contribution to the phase is the subject of the present work. Our goal—direct observation of the effects of gravity in an optical interferometric experiment—is part of the efforts to design new tests of the equivalence principle. We now review its formulation and connection to the gravitationally induced phase, and then outline the structure of the following discussion.

The Einstein equivalence principle (EEP) is the foundation of all metric theories of gravity, including general relativity [1–3,28,29]. The principle is comprised of three statements. The first—*weak equivalence principle*—states that the trajectory of a freely falling test body is independent of its internal composition. The other two statements deal with outcomes of nongravitational experiments performed in freely falling laboratories where self-gravitational effects are negligible. The second statement—*local Lorentz invariance*—asserts that such experiments are independent of the velocity of the laboratory where the experiment takes place. The third statement—*local position invariance* (LPI)—asserts that “the outcome of any local nongravitational experiment is independent of where and when in the Universe it is performed” [29].

Tests of the “when” part of the EEP bound the variability of the nongravitational constants over cosmological timescales [30–32]. The “where” part was expressed in Einstein’s analysis [33] of what in modern terms is a comparison of two identical frequency standards in two different locations in a static gravitational field. The so-called *redshift* implied by the EEP affects the locally measured frequencies of a spectral line that is emitted at location 1 with the proper frequency ω_0 and then detected at location 2 with ω' . The redshift can be parametrized as

$$\frac{\Delta\omega}{\omega_0} = (1 + \alpha)\Delta U + \mathcal{O}(c^{-3}), \quad (2)$$

where $\Delta\omega := \omega' - \omega_0$ and $\Delta U := U_2 - U_1$, where $U_i := -\phi_i^{\text{N}}/c^2$ has the opposite sign of the Newtonian gravitational

potential ϕ_i^{N} at the emission (1) and detection (2), while $\alpha \neq 0$ accounts for possible violations of LPI. In principle, α may depend on the nature of the clock that is used to measure the redshift [2,29,31]. For example, the standard model extension (SME) includes all possible Lorentz- and *CPT*-violating terms preserving the fundamental $SU(3) \times SU(2) \times U(1)$ gauge invariance and power-counting renormalizability [34]. The SME contains constrained parameters whose different combinations may lead to $\alpha \neq 0$, as well as different couplings of the Standard Model parameters and gravity [35–37].

A typical redshift experiment involves a pair of clocks, naturally occurring [38] or specially designed [39–45], whose readings are communicated by EM radiation. It should be noted that the leading term in Eq. (2) is the same in all metric theories of gravity. Evaluating $\Delta\omega/\omega_0$ to a higher order in the post-Newtonian approximation leads to expressions that depend on the specifics of the theory and are different between general relativity and alternative metric theories of gravity [2,3]. Therefore, as we detail in Sec. III, the absolute violation of LPI in terms of a single parameter is meaningfully defined in the near-Earth experiments only up to the level of 10^{-5} .

This level of precision of the measurements of α is already well-established [2,29,42,43]. Moreover, comparison of colocated ultraprecise clocks, using two different atoms (hydrogen and cesium) for their working transitions, allowed for a bound on the difference $\alpha_{\text{H}} - \alpha_{\text{Cs}}$ with the precision of 2×10^{-7} [42].

These estimations of α are based on implicit or explicit assumptions on the standard propagation of the EM radiation [37]. Furthermore, parameters of the models with dark matter directly coupling to the EM field are also constrained using atomic measurements [46]. As a matter of principle, once the possibility of LPI violation is entertained, there is no reason for it to be the same for all fields of the Standard Model, and the distinct coefficients in the symmetry-violating terms in SME are generally considered [34,35]. Hence, different types of experiments, which employ a single EM source and compare optical phase differences between beams of light traversing different paths in a gravitational field, provide a complementary test of LPI. Our analysis is purely classical. However, it can be adopted to describe the state transformation of photonic qubits.

The rest of this paper is organized as follows. The frequency shift of Eq. (2) underpins the phase difference whose extraction we outline in Sec. II. This protocol forms a novel test of the EEP exploiting a single EM source and a double large-distance interferometric measurement performed at two different gravitational potentials. Section III discusses in detail how by comparing the phase shifts obtained at a satellite and on Earth, it is possible to overcome the first-order Doppler effect and obtain the gravitational contribution. Section IV presents simulations that are based

on the orbits of existing and proposed satellites, and discusses the current technological limitations of the scheme.

II. DESCRIPTION OF THE PROPOSAL AND OF THE DOPPLER-CANCELLATION SCHEME

A possible setup for our proposal is sketched in Fig. 1 and is based on the satellite interferometry experiment realized in [16]. Such an interferometric measurement is obtained by sending a light pulse through a cascade of two fiber-based Mach-Zehnder interferometers (MZIs) of equal temporal imbalance τ_l . After the first MZI the pulse is split into two temporal modes, called *short* (S) and *long* (L) depending on the path taken in the first MZI. The equal imbalance of the two MZIs guarantees that the two pulses are recombined at the output of the second MZI, where they are detected. The combination of the possible paths the pulses may take leads to a characteristic detection pattern comprising three possible arrival times for each pulse. The first (third) peak corresponds to the pulses that took the S (L) path in both the MZIs, while the midpeak is due to the pulse that took the S path in the first interferometer and the L path in the subsequent one, or vice versa. Hence, interference is expected only in the central peak, due to the indistinguishability of the two possibilities.

Such an interference is modulated by the phase-difference φ accrued in the propagation by the two interfering paths, that depends on the relative motion between the ground station (GS) and the spacecraft (SC), as depicted in Fig. 1, and on the difference in gravitational potentials, as we will detail in the

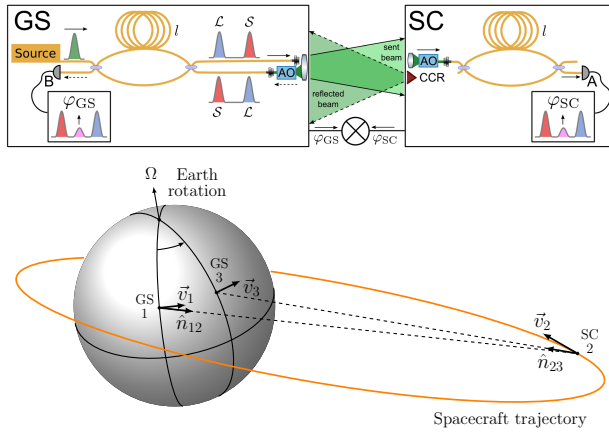


FIG. 1. Top: scheme of the proposal. Both the ground station (GS) and the spacecraft (SC) are equipped with a Mach-Zehnder interferometer (MZI) of equal delay line l and an adaptive optics (AO) system for fiber injection. Bottom: geometry of the experiment: \vec{v}_1 is the velocity of the GS at the emission at potential U_1 ; \vec{v}_2 is the velocity of the SC at the detection on the satellite at potential U_2 ; \vec{v}_3 is the velocity of the GS at the detection of the beam retroreflected by the corner-cube retroreflector (CCR) on the SC, which occurs at potential $U_3 = U_1$. Approximating Earth's angular velocity Ω as constant, $|\vec{v}_1|^2 = |\vec{v}_3|^2$. Vectors \hat{n}_{12} and \hat{n}_{23} are the Newtonian propagation directions of the light pulses.

following. From the ratio of the intensity of the central peak to the lateral ones an estimation of φ can be obtained [16]. To realize this interferometric measurement, the coherence time of the source τ_c must be, at the same time, much shorter than the temporal imbalance $\tau_l \approx \tau_l^{\text{GS}} \approx \tau_l^{\text{SC}}$ introduced by the single delay line, and longer than the mismatch $\Delta\tau_l := \tau_l^{\text{SC}} - \tau_l^{\text{GS}}$ between the two interferometers (which cannot be perfectly identical), i.e.

$$\Delta\tau_l < \tau_c \ll \tau_l. \quad (3)$$

We will show in Appendix A how the setting of the source can be chosen such that Eq. (3) is satisfied.

Furthermore, we will assume that a free-space to single-mode fiber coupling system is implemented to guarantee the spatial overlap of the interfering beams, resulting in high-interference visibility (the interferometric visibility is further discussed in Appendix D). The latter assumption seems to be very demanding from an experimental point of view. However, it was recently demonstrated that it is possible to couple into single-mode fibers a laser beam coming from satellites [47,48]. Indeed, by using an adaptive optics (AO) system [48], it is possible to correct the wavefront distortion induced by turbulence and to mitigate losses and intensity fluctuations at the receiver. We note that, as discussed below, the phase-difference φ is not affected by turbulence. More technical details on the experimental setup, attesting to the feasibility of our proposal within a decade, are given in Appendix A.

The Doppler-cancellation scheme is based on the fact that the one-way phase-difference φ_{SC} contains both the first-order Doppler shift and higher-order terms including the gravitational contribution $U_2 - U_1 \equiv U_{\text{SC}} - U_{\text{GS}}$, while the two-way phase-difference, φ_{GS} , contains only Doppler terms since the gravitational contribution is canceled out at the leading order in the two-way trip. The first-order Doppler terms are eliminated by manipulating the corresponding data sets from the GS and SC in a manner similar to the time-delay interferometry techniques in [49]. The key feature allowing for this is that the ratio of first-order Doppler terms in φ_{SC} and φ_{GS} is exactly equal to two (see below).

Hence, using the linear combination

$$S := \varphi_{\text{SC}} - \frac{1}{2}\varphi_{\text{GS}} \quad (4)$$

of the two phase differences φ_{SC} and φ_{GS} , that are obtained from an interferometric measurement of the kind described above, a bound on α will be retrieved. This procedure parallels the data processing techniques used in the Gravity Probe A experiment [50]. Here φ_{SC} is measured at detector A located on the SC, while φ_{GS} is measured at detector B located at the GS by exploiting the reflection of the sent

beam obtained with a corner-cube retroreflector (CCR) mounted on the SC (Fig. 1).

The explicit form of the signal is derived in the next section and in Appendix B, resulting in

$$\begin{aligned} \frac{S}{\omega_0 \tau_l} = & (1 + \alpha)(U_2 - U_1) + \frac{1}{2}(\beta_2^2 - \beta_1^2) \\ & + \vec{\beta}_1 \cdot (\vec{\beta}_1 - \vec{\beta}_2) - (\mathbf{d}_2 - \mathbf{d}_1)^2 - T(\hat{n}_{12} \cdot \vec{a}_1) \\ & - ((\vec{\beta}_2 - \vec{\beta}_1)^2 - (\mathbf{d}_2 - \mathbf{d}_1)^2) \frac{\tau_l}{4T}, \end{aligned} \quad (5)$$

where α parametrizes the violation of LPI, $\vec{\beta}_i := \vec{v}_i/c$, $\mathbf{d}_i := \hat{n}_{12} \cdot \vec{\beta}_i$, T is the zeroth-order time-of-flight between the GS and the SC, $\vec{a}_1 = d\vec{\beta}_1/dt$ is the centripetal acceleration of the GS at 1, and the other quantities are specified in Fig. 1.

III. PHASE-SHIFT ESTIMATION IN THE PARAMETRIZED POST-NEWTONIAN APPROXIMATION

A. Notation

We present a detailed analysis of the phases to be measured by exploiting the parametrized post-Newtonian (PPN) formalism [1–3] using the notation of [15]. The expansion order is labeled by the parameter ϵ , which is set to 1 at the end of the calculation. The PPN formalism applied to near-Earth experiments implies $\epsilon \approx 10^{-5}$, since Earth’s gravitational potential is defined to be of the order ϵ^2 and $U_\oplus = GM_\oplus/(c^2 R_\oplus) \approx 10^{-10}$ [2] (the subscript \oplus refers to Earth). It is worth noticing that the absolute value of the GS and SC velocities v_i/c are also bounded by 10^{-5} , and are thus on the order of ϵ . Another important scale parameter is given by the ratio $\mu := \tau_l/T$ between the delay-line imbalance and the zeroth-order time-of-flight. For an

imbalance of $l = 1.2$ km, as used in the following, we have $\mu \approx 10^{-3}$.

At this level of precision, we can ignore the effects of the gravitational field of other bodies in the Solar System, approximate the spacetime around the Earth as static, and consider only the leading (i.e. second order in ϵ) post-Newtonian effects. Thus, the non-vanishing components of the metric in the PPN approximation are [1–3,28]

$$g_{00} = -1 + 2U, \quad g_{ij} = \delta_{ij}(1 + 2U), \quad (6)$$

where the gravitational potential around Earth includes the quadrupole term [28]

$$U := U(r, \theta) = \frac{GM_\oplus}{c^2 r} \left(1 - \frac{1}{2} J_2 \frac{R_\oplus^2}{r^2} (3 \cos^2 \theta - 1) \right) \quad (7)$$

with $J_2 = 1.083 \times 10^{-3}$ the normalized quadrupole moment. The off-diagonal terms in the PPN-metric are of the order ϵ^3 , while the next-order correction to g_{00} is of the order ϵ^4 [2,3]. Taking these and higher-order terms into account allows to obtain the frequency-shift with arbitrary precision. Unlike the universal ϵ^2 term, the ϵ^3 and higher-order terms depend on the specific EEP-conforming metric theory used [2,3].

Unit (Euclidean) vectors \hat{n}_{ij} describing light propagation direction carry double subscripts indicating the starting (i) and ending (j) points of the geodesic segment followed by the pulse. More details on light propagation in the PPN formalism are reported in Appendix B 1.

Since we deal with short time intervals, we use an Earth-centered inertial system as the standard reference frame with coordinates (t, \vec{x}) . For brevity we refer to this system as the “global” reference frame (GRF), distinguishing it from the local frames that are established at the GS and the SC along their world lines parametrized by their proper times τ^{GS} and τ^{SC} [Fig. 2 (left)], which are distinguished by

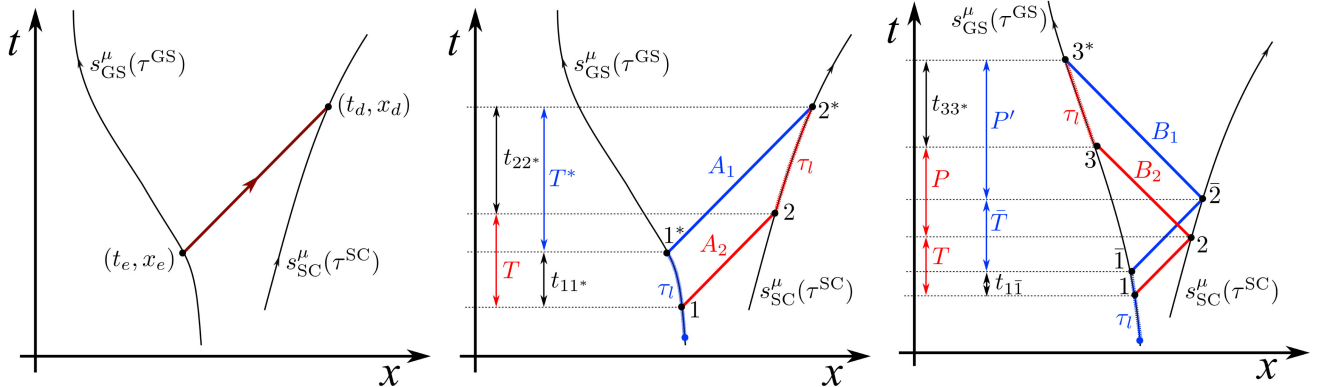


FIG. 2. Left: spacetime diagram with a single null geodesic segment connecting the emission and detection points lying along the ground station and the spacecraft worldlines (s_{GS}^μ and s_{SC}^μ , respectively). Center: spacetime diagram for the one-way phase-shift. We define: $T := t_2 - t_1$ (zeroth-order time-of-flight from the GS to the SC) and $T^* := t_{2^*} - t_{1^*}$. Right: spacetime diagram for the two-way phase-shift. We define: $\bar{T} := t_2 - t_1$, $P' := t_{3^*} - t_2$, and $P := t_3 - t_2$. The coordinates (t, x) refer to the GRF. The x -axis represents all three spatial directions.

superscripts. Quantities that are expressed in the GRF will usually carry no superscripts. On the other hand, the subscripts refer to the location of a particular event; for example 1 and 3 occur at the GS, while 2 happens at the SC (see Fig. 1). In the following calculation we use the coordinates \vec{x}_1 and \vec{x}_2 , the velocities \vec{v}_1 and \vec{v}_2 , and accelerations \vec{a}_1 and \vec{a}_2 at the points 1 and 2 and suppose the time-of-flight T is known.

Coordinate-time and proper-time intervals are defined as $t_{ij} := t_j - t_i$ and $\tau_{ij} := \tau_j - \tau_i$, respectively, and are related through the line element

$$-d\tau^2 = (-1 + 2U)dt^2 + \frac{v^2}{c^2}dt^2 + \mathcal{O}(\epsilon^3), \quad (8)$$

where τ is the proper time of a local observer (at the GS or SC) that moves with the velocity $\vec{v} = c\vec{\beta}$. Hence,

$$\tau_{ij} = \left(1 - \frac{1}{2}\beta_i^2 - U_i\right)t_{ij}, \quad (9)$$

is exact at $\mathcal{O}(\epsilon^2)$, provided that $v_i t_{ij} \lesssim \epsilon r_i$ and $a_i t_{ij} \lesssim \epsilon v_i$.

B. How to evaluate the phase shift

The most effective way to estimate the phase-shift for the interfering beams in Fig. 1 is to use the spacetime diagrams of Fig. 2 [12]. Within the geometric optics description of [1,4], the scalar amplitude of a monochromatic wave can be written as $\psi(t, \vec{x}) = A(t, \vec{x})e^{i\Phi(t, \vec{x})}$, where the phase $\Phi(t, \vec{x})$ is a scalar function satisfying the eikonal equation, which is the Hamilton-Jacobi equation for massless particles [1,4]. If we consider a single null geodesic segment that connects two points belonging to two timelike trajectories— (t_e, \vec{x}_e) and (t_d, \vec{x}_d) in Fig. 2 (left)—it follows that the accumulated phase can be evaluated indifferently at the emission (e) or detection (d) point:

$$\phi[e \rightarrow d] = \phi^{\text{GRF}}(t_d, \vec{x}_d) = \phi^{\text{GRF}}(t_e, \vec{x}_e). \quad (10)$$

Since the phase is a scalar, it can be evaluated in either the local frames established at the SC or at the GS according to

$$\begin{aligned} \phi[e \rightarrow d] &= \phi^{\text{SC}}[\tau_d^{\text{SC}}, \vec{x}_d^{\text{SC}}(\tau_d^{\text{SC}})] \\ &= \phi^{\text{GS}}[\tau_e^{\text{GS}}, \vec{x}_e^{\text{GS}}(\tau_e^{\text{GS}})] = \phi_0 - \omega_0 \tau_e^{\text{GS}}. \end{aligned} \quad (11)$$

In the above expression the form of the phase is expressed in the GS-frame. The 4-wave vector is given by $k_\mu = \partial_\mu \Phi$, and the emitted frequency is $\omega_{\text{GS}} \equiv \omega_0 = -u_{\text{GS}}^\mu k_\mu$, where u_{GS}^μ is the 4-velocity of the frame and ϕ_0 is an initial phase.

In our setting, this recipe implies to back-propagate the light trajectory from the final detection point (2^* for the one-way measurement and 3^* for the two-way one) to the GS worldline, and to take into account the presence of the delay line (of proper time τ_l) in the path [see Fig. 2].

It is worth noticing that, since the two waves associated to the two possible paths are required to interfere at the same spacetime event, the backpropagation implies that the two points where the phase is estimated at the GS are actually two different spacetime events for the two paths. Furthermore, we can apply the machinery described above to pulses of light, since they are obtained as superposition of plane waves [12].

C. One-way phase difference

The spacetime diagram of the two beams A_1 and A_2 interfering after the one-way trip at the point $2^* := (t_{2^*}, \vec{x}_{2^*})$ is represented in Fig. 2 (center). A_2 is the path followed by the pulse that leaves the GS at 1, reaches the SC at 2, and ends at 2^* by taking the delay line on the satellite just before detection. Hence, the phase-shift at point 2^* , given path A_2 , taking into account the delay line (d.l.), and the back-propagation (b.p.) is

$$\begin{aligned} \phi[A_2] &= \phi^{\text{SC}}[2^*|A_2] \\ &\stackrel{\text{d.l.}}{=} \phi^{\text{SC}}[\tau_2^{\text{SC}} := \tau_2^{\text{SC}} - \tau_l, \vec{x}_2^{\text{SC}}(\tau_2^{\text{SC}})] \\ &\stackrel{\text{b.p.}}{=} \phi^{\text{GS}}[\tau_1^{\text{GS}}, \vec{x}_1^{\text{GS}}(\tau_1^{\text{GS}})] \\ &\stackrel{(11)}{=} \phi_0 - \omega_0 \tau_1^{\text{GS}}. \end{aligned} \quad (12)$$

On the other hand, path A_1 is followed by the pulse that arrives at 2^* while leaving the GS at 1^* after having taken the delay line on the ground. Thus, its accumulated phase is

$$\begin{aligned} \phi[A_1] &= \phi^{\text{SC}}[2^*|A_1] \\ &\stackrel{\text{b.p.}}{=} \phi^{\text{GS}}[\tau_{1^*}^{\text{GS}}, \vec{x}_{1^*}^{\text{GS}}(\tau_{1^*}^{\text{GS}})] \\ &\stackrel{\text{d.l.}}{=} \phi^{\text{GS}}[\tau_{1^*}^{\text{GS}} - \tau_l, \vec{x}_{1^*}^{\text{GS}}(\tau_{1^*}^{\text{GS}} - \tau_l)] \\ &\stackrel{(11)}{=} \phi_0 - \omega_0(\tau_{1^*}^{\text{GS}} - \tau_l). \end{aligned} \quad (13)$$

The phase-difference for the one-way measurement performed at the SC is

$$\varphi_{\text{SC}} := \phi[A_2] - \phi[A_1] = \omega_0(\tau_{1^*}^{\text{GS}} - \tau_1^{\text{GS}} - \tau_l), \quad (14)$$

where $\tau_{1^*}^{\text{GS}} - \tau_1^{\text{GS}} \equiv \tau_{11^*}^{\text{GS}}$ is related to coordinate time interval t_{11^*} by Eq. (9) and

$$t_{11^*} + T^* = T + t_{22^*} \quad (15)$$

holds, with $\tau_{22^*}^{\text{SC}} \equiv \tau_l$. In the Appendix B 2 we evaluate φ_{SC} by expanding the unknown quantities in powers of ϵ (these are the time-of-flight T^* of the delayed pulse, its Newtonian propagation direction $\hat{n}_{1 \rightarrow 2^*}$, and the coordinate-time interval t_{11^*}) and by using the equations describing the motion of the SC and the light propagation in the PPN approximation. We obtain

$$\varphi_{\text{SC}} = -\omega_0 T_1 + \varphi_{\text{SC}}^{(2)}, \quad (16)$$

where the first-order Doppler correction is given by

$$T_1 = \hat{n}_{12} \cdot (\vec{\beta}_2 - \vec{\beta}_1) \tau_l. \quad (17)$$

The detailed calculation and the explicit form of the second-order term $\varphi_{\text{SC}}^{(2)}$ are given in Appendix B 2.

D. Two-way phase difference

The spacetime diagram of the two beams B_1 and B_2 interfering after the two-way trip at the spacetime event $3^* := (t_{3^*}, \vec{x}_{3^*})$ is represented in Fig. 2 (right). Analogously to the one-way shift, for the B_2 path (delay line on the ground just before detection) we have that

$$\begin{aligned} \phi[B_2] &= \phi^{\text{GS}}[3^*|B_2] \\ &\stackrel{\text{d.l.}}{=} \phi^{\text{GS}}[\tau_3^{\text{GS}} := \tau_{3^*}^{\text{GS}} - \tau_l, \vec{x}^{\text{GS}}(\tau_3^{\text{GS}})] \\ &\stackrel{\text{b.p.}}{=} \phi^{\text{GS}}[\tau_1^{\text{GS}}, \vec{x}^{\text{GS}}(\tau_1^{\text{GS}})] \\ &\stackrel{(11)}{=} \phi_0 - \omega_0 \tau_1^{\text{GS}}, \end{aligned} \quad (18)$$

while for the path B_1 (delay line on the ground at the start) we have that

$$\begin{aligned} \phi[B_1] &= \phi^{\text{GS}}[3^*|B_1] \\ &\stackrel{\text{b.p.}}{=} \phi^{\text{GS}}[\tau_1^{\text{GS}}, \vec{x}^{\text{GS}}(\tau_1^{\text{GS}})] \\ &\stackrel{\text{d.l.}}{=} \phi^{\text{GS}}[\tau_1^{\text{GS}} - \tau_l, \vec{x}^{\text{GS}}(\tau_1^{\text{GS}} - \tau_l)] \\ &\stackrel{(11)}{=} \phi_0 - \omega_0 (\tau_1^{\text{GS}} - \tau_l). \end{aligned} \quad (19)$$

Hence, the phase difference for the two-way measurement realized at the GS is given by

$$\varphi_{\text{GS}} := \phi[B_2] - \phi[B_1] = \omega_0 (\tau_1^{\text{GS}} - \tau_1^{\text{GS}} - \tau_l), \quad (20)$$

where $\tau_1^{\text{GS}} - \tau_1^{\text{GS}} \equiv \tau_{1\bar{1}}^{\text{GS}}$ is related to $t_{1\bar{1}}$ by Eq. (9), and

$$t_{1\bar{1}} + \bar{T} + P' = T + P + t_{33^*}. \quad (21)$$

with $\tau_{33^*}^{\text{GS}} \equiv \tau_l$. With a procedure analogous to the one of the one-way phase-shift, we finally obtain

$$\varphi_{\text{GS}} = -2\omega_0 T_1 + \varphi_{\text{GS}}^{(2)}, \quad (22)$$

where $\varphi_{\text{GS}}^{(2)}$ and the detailed calculation are explicitly given in the Appendix B 3.

The first-order term $\varphi_{\text{GS}}^{(1)} := -2\omega_0 T_1$ is exactly what has been measured in [16]. As anticipated above, the ratio of the first-order terms in φ_{SC} and φ_{GS} is exactly two, thus

allowing for the Doppler-cancellation strategy that is summarized in Eq. (4).

The effects of the length mismatch between the loops are the main practical limitation of the scheme and are discussed in Appendix C.

IV. SIMULATIONS

We present the numerical estimation of the signal in Eq. (5) by exploiting the orbit of existing and simulated satellites, covering a wide range of orbital parameters. The first two satellites are currently used by the International Laser Ranging Service (ILRS) [51]. The satellite laser ranging (SLR) technique allows for a high-accuracy estimation of the distance of such satellites by measuring the time-of-flight of laser pulses that are sent from a GS on Earth, then retroreflected by the CCRs mounted on the orbiting terminal, and finally collected by the same GS. ILRS makes available the consolidated prediction format [52] files for SLR orbit, containing the geocentric (inertial Earth-centered) position of the satellites at a given time. We chose to perform the simulation using two satellites placed in different orbits: Ajisai (circular orbit) and Galileo 201 (eccentric orbit). In particular, Ajisai has an altitude of about 1500 km, as used in the estimation of the expected gravitational phase-shift after Eq. (1). The used GS is the Matera Laser Ranging Observatory (MLRO) [53] of the Italian Space Agency, that was exploited for various demonstrations of the feasibility of satellite quantum communications [16,17,25,54–57].

Two other simulations use satellites that are placed on a highly eccentric elliptical orbit, known as Molniya orbit. This orbit is well suited for telecommunications in polar regions and has therefore been exploited by the Soviet Union for placing its satellites. Satellites on these orbits spend most of their time close to the apogee, with rapid passages at the perigee. We specialized our analysis on the Molniya 1-87 satellite [58], whose orbit has an inclination of 63.6° and an eccentricity of 0.68. Since all existing satellites placed on Molniya orbits are visible from the northern hemisphere only at perigee, we decided to simulate the orbit of a Molniya-like satellite spending most its time above the southern hemisphere and passing on top of the MLRO at the apogee (called S-Molniya).

All the orbits are simulated using the open source Orekit space dynamics library [59], that can both simulate an orbit starting from the two-line elements (TLE) or the Keplerian orbital parameters and reproduce real passages as seen from an actual GS on Earth.

The upper panels of Fig. 3 show the signal $S/(\omega_0 \tau_l)$ from Eq. (5) as a function of the time passage for the satellites, while the bottom panel are the signals estimated by supposing that such terminals are equipped with an interferometer providing a delay line of $l = 1.2$ km (so $n = 1.5$ implies $\tau_l \approx 6 \mu\text{s}$) and that the initial wavelength is

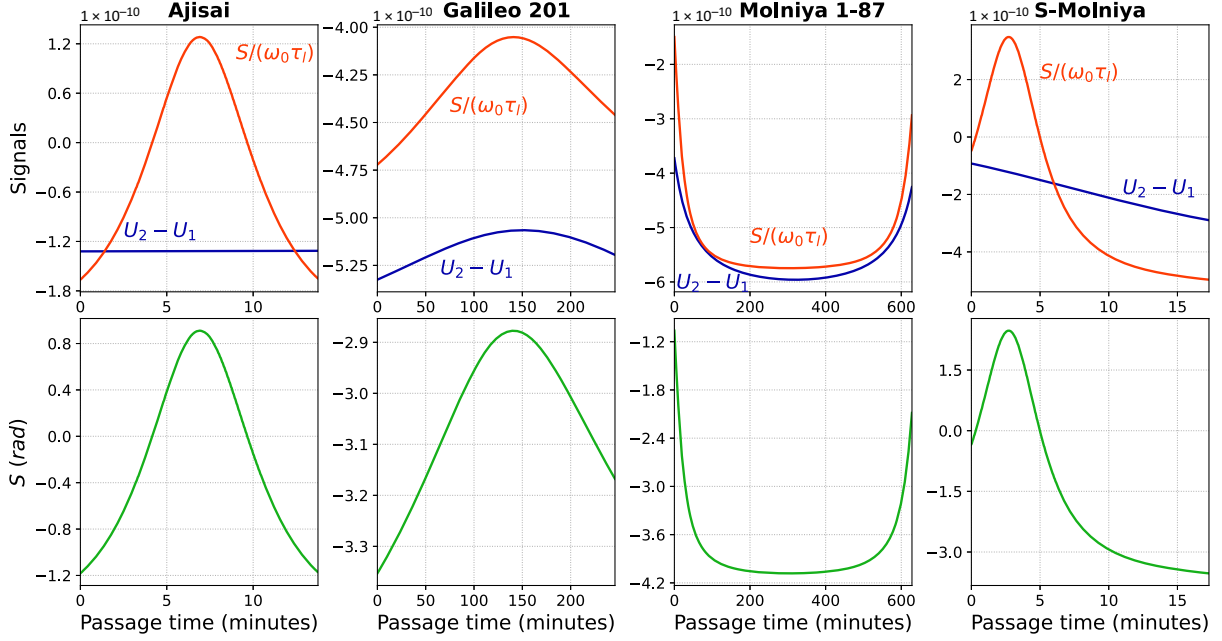


FIG. 3. Results obtained with, from left to right, Ajisai (inclination 50° , eccentricity 0.001, altitude 1490 km), Galileo 201 (inclination 50° , eccentricity 0.158, altitude ranging from 17,000 km to 26,210 km), Molniya 1-87 (inclination 63.6° , eccentricity 0.68, altitude ranging from 2000 to 38,000 km) and an hypothetical satellite on a South Pole Molniya-like orbit (the same parameters as Molniya 1-87, but with perigee on the northern hemisphere) seen from MLRO. Upper panels show the signals $\Delta U = U_2 - U_1$ and $S/(\omega_0\tau_l)$ from Eq. (5) (with $\alpha = 0$) as a function of the passage time. Bottom panels show the signal S expected with a delay line and wavelength $\lambda = 1550$ nm.

$\lambda = 2\pi c/\omega_0 = 1550$ nm. This choice of the parameters τ_l and ω_0 brings the strength of the signal in Eq. (5) into a measurable regime on the order of a few radians.

While the signal $S/(\omega_0\tau_l)$ is of the same order of magnitude for all the orbits, very low-eccentricity orbits for which $\Delta U = U_2 - U_1 \approx \text{const}$ (e.g., Ajisai) are not suitable in practice, since the lack of variability in ΔU prevents its separation from the constant offset $\omega_0\tau_l\delta_l$ that is due to the mismatch $\delta_l := (\tau_l^{\text{SC}} - \tau_l^{\text{GS}})/\tau_l^{\text{GS}}$ of the delay lines, as discussed in Appendix C.

V. CONCLUSIONS

Our proposal allows for the cancellation of the first-order Doppler effect in optical redshift experiments. However, this proposal still faces two important practical issues. First, atmospheric turbulence is a limiting factor for large-distance optical interferometry. However, the planned temporal delay between the two pulses is four orders of magnitude lower than the conventional millisecond threshold of the turbulence correlation time [60]. As a result, both the interfering beams suffer through the same random noise that is canceled in measuring φ_{SC} and φ_{GS} . In fact, the same scale difference was successfully exploited in [16].

Second, the two delay lines cannot be perfectly identical. However, by exploiting commercially available fiber stretchers at each MZI and by monitoring in real-time

the first-order interference with a stabilization laser of long coherence time (see Appendix A for more details), it is possible to phase-stabilize the two MZIs and achieve a relative precision δ_l of the order of 10^{-6} , which for $l = 1.2$ km translates into an absolute difference of 1 mm. It is worth noting that the capability of controlling the relative length of two arms of 1 km balanced interferometer with a precision of 1 mm has been reported in [61], and this technique can be adapted to unbalanced interferometers, provided an appropriate frequency reference is supplied to the two terminals (see Appendix A). In this case the measured signal gets a constant offset $\omega_0\tau_l\delta_l$, that can be reliably estimated and eliminated by using SLR data. Moreover, the additional variable term of the order δ_l can be eliminated similarly to the second-order Doppler terms (see Appendix C).

Concluding, in this work we propose an optical scheme to suppress the first-order Doppler effect in order to measure the gravitational redshift with satellite systems. The possibility of testing gravitational physics using optical interferometric measurements between moving terminals represents an important point in the study of Einstein's theory and can lead to new tests of its interplay with quantum mechanics through the exploitation of quantum optical effects. The recent advancements in satellite optical technologies make this proposal both attractive and feasible with current technologies.

ACKNOWLEDGMENTS

The work of D. R. T. is supported by Grants No. FA2386-17-1-4015 of AOARD and No. FA2386-20-1-4016. A. R. H. S. was supported by the Natural Sciences and Engineering Research Council of Canada and the Dartmouth College Society of Fellows. F. V. thanks Costantino Agnesi for useful discussions. We acknowledge the International Laser Ranging Service (ILRS) for SLR data and software.

APPENDIX A: MORE DETAILS ON THE EXPERIMENTAL SETUP

Here we provide some experimental details in order to attest to the feasibility of our proposal. First, we address the problem of stabilizing two strongly unbalanced MZI under the assumption that the length of the two delay lines can be kept equal at the required precision. Second, since the MZIs have to be implemented with single-mode fibers to allow for strong imbalances and to achieve a good overlap of the interfering beams, we will sketch a possible single-mode fiber-injection system exploiting adaptive optics. It is worth noticing that the proposed system is feasible with current technology given the maturity of fiber components at 1550 nm.

1. Details of the interferometers

The MZI of both terminals employ two optical fibers (where one is a fiber spool much longer than the other) sandwiched between two 50/50 fiber beam splitters. In addition, one arm of the interferometer is equipped with a fiber stretcher (f.s.) in order to finely tune the imbalance to $l = 1.2$ km. Note that a suitable laser emitting pulses with short coherence time (≈ 1 ps) can be employed before the launch to ensure that the relative imbalance between the two delay lines is of the order of 1 mm, by measuring the imbalance δl of the single MZI [17] with high-resolution superconducting nanowire single-photon detectors (SNSPDs). It is worth noting that commercial fiber stretchers can provide down to 0.1 μm of minimum step, so that, in principle, $\delta l/l \approx 10^{-10}$.

To phase-stabilize the MZIs and keep the relative imbalances between the two to the required precision of $\delta l = \Delta\tau_l/\tau_l \approx 10^{-6}$, an auxiliary stabilization (S) laser with central frequency ν_S and bandwidth $\Delta\nu_S$ is employed at each terminal to monitor in real-time the first-order interference. The stabilization laser is assumed to be characterized by a coherence time τ_c^S much longer than the target imbalance τ_l , hence $\tau_c^S \gg \tau_l$. For example, since $\tau_l = 6$ μs , a laser with a bandwidth of $\Delta\nu_S \ll 1/\sqrt{4\pi\tau_l^2} \approx 50$ kHz at a wavelength of 1560 nm is suitable for this task. With such a stabilization laser one can lock the optical phase of the interferometer with a precision of the order of $\Delta\nu_S/\nu_S \approx 10^{-10}$.

Given the system described above, it is possible to ensure that the relative mismatch of the SC's delay line (τ_l^{SC}) the GS's delay line ($\tau_l^{GS} \equiv \tau_l$) is at most $\delta_l = \Delta\tau_l/\tau_l \approx 10^{-6}$. Having fixed $\tau_l = 6$ μs , we have that $\Delta\tau_l \approx 10$ ps, and we can define the parameters of the signal source by requiring that 10 ps $< \tau_c \ll 1$ μs to fulfill Eq. (3). Hence, a suitable signal source is a 1550 nm fiber-coupled laser with a repetition rate of 100 Hz, average power of 10 W (energy pulse of 100 mJ), coherence time τ_c of 10 ns, and linewidth of $\Delta\nu \approx 37.5$ MHz. Recent experiments have demonstrated that such a source is feasible with current technology [62,63]. In order to reach the required optical precision $\delta\varphi_{gr} \approx 10$ μrad , it is necessary to detect $N \gtrsim 1/\delta\varphi_{gr}^2 \approx 10^{10}$ photons. Since a 100 mJ pulse at 1550 nm contains approximately 8×10^{17} photons, the system can work with losses up to almost 80 dB. Note that standard fibers at 1550 nm introduce a tolerable amount of losses even with strong imbalances, since the attenuation coefficient is about 0.2 dB/km at this wavelength. In order to achieve the required signal-to-noise ratio, it is necessary to use a low noise InGaAs photodiode.

2. Details of the fiber-injection system

The free-space propagation of light through turbulent atmosphere affects the quality of the beam wavefront, which has to be corrected before being coupled to the SMF. To accomplish such a task we envisage to use an adaptive optics system like the one implemented in [48] and sketched in Fig. 4.

This system is based on the exploitation of an additional beacon laser at a wavelength a few nanometers apart from the signal one (e.g., 1545 nm). This additional beam shares the same free-space optical path of the signal beam, and is used as feedback for the adaptive optics system. At the detection, the beacon beam can be filtered out from the signal beam by using wavelength-division-multiplexer (WDM) filters, which provide down to 0.1 nm of bandwidth separation. Figure 4 shows the expansion of the closed-loop adaptive optics box introduced in the top panel of Fig. 1. The input (In) of the AO system is the aberrated beam wavefront collected by a telescope (sketched as a

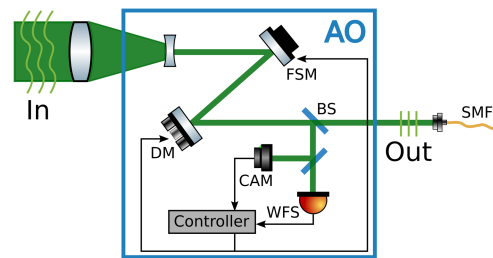


FIG. 4. AO system needed for the free-space to SMF coupling. The beam splitter (BS) can be replaced by a dichroic mirror if the beacon laser has a different wavelength than the signal beam.

lens), while the output (Out) is the corrected and collimated beam to be coupled to the SMF. The first element of the AO box is a lens whose focal length is chosen in order to reduce and collimate the incoming beam. The light is then reflected by a fast steering mirror (FSM) and a deformable mirror (DM) before passing a beam splitter (BS). The transmitted path exits from the AO box and provides the collimated and corrected beam to be coupled to the SMF, while the reflected path is collected by a camera (CAM) and a wave front sensor (WFS). The CAM could be a camera or a position-sensitive-detector to measure the wandering of the beam at the focal plane and thus the low-order tilt due to turbulence, while the WFS could be a Shack-Hartmann sensor or a self-referenced interferometer to estimate the higher-order aberrations. The two signals generated by the CAM and the WFS drive the FSM and the DM in order to correct for low- and high-order aberrations of the wavefront.

The actual parameters of the AO box must be carefully chosen and they depend primarily on the level of expected turbulence, the dimensions of the beams, the optical power collected by the telescope and the velocity of the closed loop. In our scheme the working parameters of the two AO systems, one at the SC and the other at the GS, will be quite different, since the first has to correct the upgoing beam sent from the GS to the SC (about 40 dB of losses in a realistic scenario), while the other must be optimized for the go and return two-way path (about 80 dB of losses). However, since the AO system exploits an additional beacon beam, the required optical power is not an actual limitation for it to work.

As noticed in [64], with long distance uplink propagation ($\gtrsim 1000$ km) the turbulence coherence area at the satellite receiver is much larger than the typical receiver aperture size. In these cases, only a tip/tilt correction without AO on the satellite is sufficient for an optimal coupling into the single-mode fiber.

Since the optical payload of the SC and the required electronics comprise commercially available devices and telecom-compatible fiber technology, we can envisage that our proposal is feasible within a decade and with no prohibitive costs.

APPENDIX B: LIGHT PROPAGATION IN THE LEADING-ORDER PPN FORMALISM AND DETAILED CALCULATION OF THE SIGNAL

We first review the essential formulas describing light propagation in the post-Newtonian approximation and then evaluate the phase differences for the one-way and two-way trips described in the main text. To simplify the notation, we use the convention $G = c = 1$, and write M instead of M_{\oplus} . Some intermediate expressions contain explicit factors of ϵ to make the separation of orders more transparent. These are set to unity at the end of the calculation.

1. Summary of the post-Newtonian results

An extended treatment of light propagation in the PPN formalism can be found in [2,3]. Light-ray trajectories from $(t_{\text{in}}, \vec{x}_{\text{in}})$ to (t, \vec{x}) (with PPN parameter $\gamma = 1$) are parametrized as

$$\vec{x}(t) = \vec{x}_{\text{in}} + \hat{n}(t - t_{\text{in}}) + \vec{x}^{(2)}(t), \quad (\text{B1})$$

where $\vec{x}^{(2)}(t)$ is the correction to the Newtonian straight propagation and the boundary condition gives $\vec{x}^{(2)}(t_{\text{in}}) = 0$. Splitting $\vec{x}^{(2)}(t)$ into its parallel and perpendicular component relative to \hat{n} as

$$\vec{x}_{\parallel}^{(2)}(t) := [\hat{n} \cdot \vec{x}^{(2)}(t)]\hat{n} \equiv x_{\parallel}^{(2)}(t)\hat{n}, \quad (\text{B2})$$

$$\vec{x}_{\perp}^{(2)}(t) := \vec{x}^{(2)}(t) - \vec{x}_{\parallel}^{(2)}(t), \quad (\text{B3})$$

then the two equations

$$\frac{dx_{\parallel}^{(2)}}{dt} = -2U, \quad (\text{B4})$$

$$\frac{d^2\vec{x}_{\perp}^{(2)}}{dt^2} = 2\nabla U - 2\hat{n}(\hat{n} \cdot \nabla U), \quad (\text{B5})$$

supplemented by the initial condition $d\vec{x}^{(2)}(t_{\text{in}})/dt = 0$, serve as a basis for the subsequent calculations.

The gravitational potential of a pointlike Earth can be approximated by

$$U \approx U(r) := \frac{M_{\oplus}}{|\vec{x}_{\text{in}} + \hat{n}(t - t_{\text{in}})|} \equiv \frac{M_{\oplus}}{r}, \quad (\text{B6})$$

yielding

$$\frac{d\vec{x}^{(2)}}{dt} = -2U(r)\hat{n} - 2\frac{M\vec{d}}{d^2} \left(\frac{\vec{x} \cdot \hat{n}}{r} - \frac{\vec{x}_{\text{in}} \cdot \hat{n}}{r_{\text{in}}} \right), \quad (\text{B7})$$

where

$$\vec{d} := \hat{n} \times (\vec{x}_{\text{in}} \times \hat{n}) = \vec{x}_{\text{in}} - (\hat{n} \cdot \vec{x}_{\text{in}})\hat{n}, \quad (\text{B8})$$

is the vector joining the center of the Earth and the point of closest approach of the unperturbed ray. Substituting Eq. (B1) into Eq. (B7) and integrating from t_{in} to t yields

$$\begin{aligned} \vec{x}^{(2)}(t) = & -2M\hat{n} \ln \frac{(t - t_{\text{in}}) + \hat{n} \cdot \vec{x}_{\text{in}} + r(t)}{\hat{n} \cdot \vec{x}_{\text{in}} + r_{\text{in}}} \\ & - 2\frac{M\vec{d}}{d^2} \left(r(t) - r_{\text{in}} - \frac{\vec{x}_{\text{in}} \cdot \hat{n}}{r_{\text{in}}}(t - t_{\text{in}}) \right). \end{aligned} \quad (\text{B9})$$

2. Light propagation for the one-way trips

Here we derive the phase φ_{SC} to order ϵ^2 . The setup is depicted in Fig. 2 (center). The main quantity of interest is thus $\tau_{11^*}^{\text{GS}}$, which is related to the global time interval t_{11^*} via Eq. (9) as

$$\tau_{11^*}^{\text{GS}} = t_{11^*} \left(1 - \frac{1}{2} v_1^2 - U_1 \right), \quad (\text{B10})$$

where the rearranged Eq. (15) gives

$$t_{11^*} = T + t_{22^*} - T^*. \quad (\text{B11})$$

Using the coincidence of the beams A_1 and A_2 at (t_2^*, \vec{x}_2^*) , the phase is expressed only in terms of the quantities that are observed at the events 1 and 2.

With the precision of $\mathcal{O}(\epsilon^2)$, the trajectory of the SC is

$$\vec{x}_{\text{SC}}(t) = \vec{x}_2 + \vec{v}_2(t - t_2) + \frac{1}{2} \vec{a}_2(t - t_2)^2 + \mathcal{O}(\epsilon^3), \quad (\text{B12})$$

hence by using Eq. (9) we find

$$\vec{x}_{2^*} := \vec{x}_{\text{SC}}(t_2^*) = \vec{x}_2 + \vec{v}_2 \tau_l + \frac{1}{2} \vec{a}_2 \tau_l^2 + \mathcal{O}(\epsilon^3). \quad (\text{B13})$$

Similarly, the trajectory of the GS is

$$\vec{x}_{\text{GS}}(t) = \vec{x}_1 + \vec{v}_1(t - t_1) + \frac{1}{2} \vec{a}_1(t - t_1)^2 + \mathcal{O}(\epsilon^3), \quad (\text{B14})$$

and so

$$\vec{x}_{1^*} := \vec{x}_{\text{GS}}(t_{1^*}) = \vec{x}_1 + \vec{v}_1 t_{11^*} + \frac{1}{2} \vec{a}_1 t_{11^*}^2 + \mathcal{O}(\epsilon^3). \quad (\text{B15})$$

We comment on the relative importance of various terms at the end of this section.

The quantities T^* and t_{11^*} are expanded in powers of ϵ

$$T^* = T + \epsilon T_1 + \epsilon^2 T_2, \quad (\text{B16})$$

$$t_{11^*} = \tau_l + \epsilon \delta_1 + \epsilon^2 \delta_2. \quad (\text{B17})$$

Using Eq. (9) again we find that with the required precision

$$\tau_l \equiv \tau_{22^*}^{\text{SC}} = t_{22^*} \left(1 - \frac{1}{2} v_2^2 - U_2 \right), \quad (\text{B18})$$

so that

$$t_{22^*} = \tau_l \left(1 + \frac{1}{2} v_2^2 + U_2 \right), \quad (\text{B19})$$

and using Eq. (B11) the relations

$$\delta_1 = -T_1, \quad (\text{B20})$$

$$\delta_2 = -T_2 + \tau_l \left(\frac{1}{2} v_2^2 + U_2 \right), \quad (\text{B21})$$

are established.

For the emission from the GS we find the closest approach vector in Eq. (B9) is $\vec{d} = \vec{x}_{\text{GS}}$, with \vec{x}_{in} being \vec{x}_1 and \vec{x}_{1^*} for the respective pulses. The pulse A_2 starts at $\vec{x}_{\text{in}} = \vec{x}_1$, hence

$$\vec{x}_2 = \vec{x}_1 + \hat{n}_{12} T + \vec{\chi}_{\uparrow}(\vec{x}_1, \hat{n}_{12}, T), \quad (\text{B22})$$

where we rewrote the $\mathcal{O}(\epsilon^2)$ terms coming from Eq. (B9) as

$$\begin{aligned} \vec{\chi}_{\uparrow}(\vec{x}_1, \hat{n}_{12}, T) := & -2M\hat{n}_{12} \ln \frac{T + \hat{n}_{12} \cdot \vec{x}_1 + |\vec{x}_1 + \hat{n}_{12} T|}{\hat{n}_{12} \cdot \vec{x}_1 + r_1} \\ & - 2 \frac{M\vec{d}_1}{d_1^2} \left(|\vec{x}_1 + \hat{n}_{12} T| - r_1 - \frac{\hat{n}_{12} \cdot \vec{x}_1}{r_1} T \right), \end{aligned} \quad (\text{B23})$$

with $\vec{d}_1 = \hat{n}_{12} \times (\vec{x}_1 \times \hat{n}_{12})$. The structure of this second-order term ensures that it will cancel with its respective counterparts in the key expressions below.

The delayed pulse A_1 leaves the GS at 1^* in the Euclidean direction

$$\hat{n}_{1^*2^*} = \hat{n}_{12} + \epsilon \vec{v}_1^* + \epsilon^2 \vec{v}_2^*. \quad (\text{B24})$$

As it is required to have unit length, the corrections to \hat{n}_{12} satisfy

$$\hat{n}_{12} \cdot \vec{v}_1^* = 0, \quad 2\hat{n}_{12} \cdot \vec{v}_2^* + v_1^{*2} = 0. \quad (\text{B25})$$

Using the parameters specifying its trajectory and noting that $r_1 \equiv r_{1^*}$, as well as that the post-Newtonian corrections to the light trajectory are already of the order of ϵ^2 —so that the corrections due to difference in $\hat{n}_{1^*2^*}$ and T^* from \hat{n}_{12} and T , respectively, are of the order ϵ^3 and can be ignored—it follows that

$$\begin{aligned} \vec{x}_{2^*} = & \vec{x}_{1^*} + \hat{n}_{1^*2^*} T^* + \vec{\chi}_{\uparrow}(\vec{x}_1, \hat{n}_{12}, T) \\ = & \vec{x}_1 + \vec{v}_1 t_{11^*} + \frac{1}{2} \vec{a}_1 t_{11^*}^2 + \hat{n}_{1^*2^*} T^* + \vec{\chi}_{\uparrow}(\vec{x}_1, \hat{n}_{12}, T). \end{aligned} \quad (\text{B26})$$

To find T^* and $\hat{n}_{1^*2^*}$ up to the second order using only quantities at the events 1 and 2, we match Eq. (B13)—using \vec{x}_2 given by Eq. (B22)—with Eq. (B26). As a result

$$\hat{n}_{12} T + \vec{v}_2 \tau_l + \frac{1}{2} \vec{a}_2 \tau_l^2 = \vec{v}_1 t_{11^*} + \frac{1}{2} \vec{a}_1 t_{11^*}^2 + \hat{n}_{1^*2^*} T^*. \quad (\text{B27})$$

Expanding it order-by-order in ϵ results in the final six equations

$$\vec{v}_2\tau_l = \vec{v}_1\tau_l + \hat{n}_{12}T_1 + \vec{v}_1^*T, \quad (\text{B28})$$

and

$$\frac{1}{2}\vec{a}_2\tau_l^2 = -\vec{v}_1T_1 + \frac{1}{2}\vec{a}_1\tau_l^2 + \vec{v}_2^*T + \vec{v}_1^*T_1 + \hat{n}_{12}T_2, \quad (\text{B29})$$

where we used Eq. (B20). Using the first of the relations (B25) with (B28) results in

$$T_1 = \hat{n}_{12} \cdot (\vec{v}_2 - \vec{v}_1)\tau_l = (\mathbf{d}_2 - \mathbf{d}_1)\tau_l, \quad (\text{B30})$$

and

$$\vec{v}_1^* = (\vec{v}_2 - \vec{v}_1)\frac{\tau_l}{T} - \hat{n}_{12}\frac{T_1}{T} = \frac{\tau_l}{T}((\vec{v}_2 - \vec{v}_1) - \hat{n}_{12}(\mathbf{d}_2 - \mathbf{d}_1)), \quad (\text{B31})$$

where $\mathbf{d}_k := \hat{n}_{12} \cdot \vec{v}_k$. We see that $T_1/T \sim |\vec{v}_1^*| = \mathcal{O}(\epsilon\mu)$.

Using the second of the relations (B25) after taking the inner product of \hat{n}_{12} with both sides of Eq. (B29) results in

$$\begin{aligned} T_2 &= \frac{1}{2}\hat{n}_{12} \cdot (\vec{a}_2 - \vec{a}_1)\tau_l^2 + \mathbf{d}_1T_1 + \frac{1}{2}\nu_1^2T \\ &= \frac{1}{2}(\mathbf{a}_2 - \mathbf{a}_1)\tau_l^2 + \mathbf{d}_1(\mathbf{d}_2 - \mathbf{d}_1)\tau_l \\ &\quad + \frac{\tau_l^2}{2T}((\vec{v}_2 - \vec{v}_1)^2 - (\mathbf{d}_2 - \mathbf{d}_1)^2), \end{aligned} \quad (\text{B32})$$

where $\mathbf{a}_k := \hat{n}_{12} \cdot \vec{a}_k$, and

$$\vec{v}_2^* = \left(\frac{1}{2}\vec{a}_2\tau_l^2 + \vec{v}_1T_1 - \frac{1}{2}\vec{a}_1\tau_l^2 - \vec{v}_1^*T_1 - \hat{n}_{12}T_2 \right) / T. \quad (\text{B33})$$

Note that in our setting the second term on the right-hand side of Eq. (B32) dominates the other two by a factor of the order $T/\tau_l = \mu^{-1} \approx 10^3$. Even so, the subdominant terms are an order of magnitude larger than ϵ^3 , and hence should be kept. The terms proportional to τ_l^2 are absent from the expressions in [12] where it was assumed that $\tau_l \lesssim \epsilon$.

Using Eqs. (B20) and (B21) we get

$$\begin{aligned} t_{11^*} &= \tau_l + \delta_1 + \delta_2 \\ &= \tau_l - T_1 - T_2 + \tau_l \left(\frac{1}{2}v_2^2 + U_2 \right) \\ &= \tau_l \left(1 + \frac{1}{2}v_2^2 + U_2 \right) - T_1 - T_2, \end{aligned} \quad (\text{B34})$$

which is related to $\tau_{11^*}^{\text{GS}}$ by Eq. (B10). Hence,

$$\tau_{11^*}^{\text{GS}} - \tau_l = -T_1 + \tau_l \left(\frac{1}{2}(v_2^2 - v_1^2) + U_2 - U_1 \right) - T_2, \quad (\text{B35})$$

where the term T_1 is responsible for the first-order Doppler effect in the phase difference at the SC

$$\varphi_{\text{SC}} = \omega_0(\tau_{11^*}^{\text{GS}} - \tau_l) = -\omega_0T_1 + \varphi_{\text{SC}}^{(2)} \quad (\text{B36})$$

with

$$\varphi_{\text{SC}}^{(2)} = \omega_0\tau_l \left(\frac{1}{2}(v_2^2 - v_1^2) + U_2 - U_1 - T_2/\tau_l \right). \quad (\text{B37})$$

3. Light propagation for the two-way trips

Here we derive the phase φ_{GS} to order ϵ^2 . The setup is depicted on Fig. 2 (right). The main quantity of interest is now $\tau_{1\bar{1}}^{\text{GS}}$, which is related to the global time interval $t_{1\bar{1}}$ via Eq. (9), where the rearranged Eq. (21) gives

$$t_{1\bar{1}} = T - \bar{T} + P - P' + t_{33^*} \quad (\text{B38})$$

Using coincidence of the beams B_1 and B_2 at (t_{3^*}, \vec{x}_{3^*}) the phase is expressed only in terms of quantities that are observed at the events 1 and 2.

4. Definition of the relevant quantities

The relevant parameters for the $2 \rightarrow 3$ part of the B_2 trajectory are the propagation direction

$$\hat{n}_{23} = -\hat{n}_{12} + \epsilon\vec{v}_1 + \epsilon^2\vec{v}_2, \quad (\text{B39})$$

that satisfies the relations

$$\hat{n}_{12} \cdot \vec{v}_1 = 0, \quad -2\hat{n}_{12} \cdot \vec{v}_2 + \nu_1^2 = 0, \quad (\text{B40})$$

and the time-of-flight from the SC to the GS

$$P = T + \epsilon\Delta_1 + \epsilon^2\Delta_2. \quad (\text{B41})$$

In general the pulse B_1 departs at the moment $t_{\bar{1}} \neq t_{1^*}$. The difference in the times of departure between B_1 and B_2 in the global time frame can be decomposed as

$$t_{1\bar{1}} = \tau_l + \epsilon\bar{\delta}_1 + \epsilon^2\bar{\delta}_2, \quad (\text{B42})$$

while the position of the GS at the moment $t_{\bar{1}}$ is

$$\vec{x}_{\bar{1}} = \vec{x}_1 + \vec{v}_1t_{1\bar{1}} + \frac{1}{2}\vec{a}_1t_{1\bar{1}}^2. \quad (\text{B43})$$

The flight time from $\bar{1}$ to $\bar{2}$ is

$$t_{\bar{1}\bar{2}} = \bar{T} = T + \epsilon\bar{T}_1 + \epsilon^2\bar{T}_2, \quad (\text{B44})$$

and the launch direction is given by

$$\hat{n}_{\bar{1}\bar{2}} = \hat{n}_{12} + \epsilon\vec{v}_1 + \epsilon^2\vec{v}_2. \quad (\text{B45})$$

The pulse reflected at t_2 is directed along

$$\hat{n}_{23^*} = -\hat{n}_{12} + \epsilon \vec{v}'_1 + \epsilon^2 \vec{v}'_2, \quad (\text{B46})$$

and the travel takes

$$P' = T + \epsilon \Delta'_1 + \epsilon^2 \Delta'_2. \quad (\text{B47})$$

The normalization conditions for the direction vectors result in

$$\hat{n}_{12} \cdot \vec{v}_1 = 0, \quad 2\hat{n}_{12} \cdot \vec{v}_2 + \vec{v}_1^2 = 0, \quad (\text{B48})$$

$$\hat{n}_{12} \cdot \vec{v}'_1 = 0, \quad -2\hat{n}_{12} \cdot \vec{v}'_2 + \nu_1^2 = 0. \quad (\text{B49})$$

Equation (B38) relates the first- and the second-order terms of the various time intervals. From Eq. (9) we have

$$\tau_l \equiv \tau_{33^*}^{\text{GS}} = t_{33^*} \left(1 - \frac{1}{2} v_1^2 - U_1 \right), \quad (\text{B50})$$

so that

$$t_{33^*} = \tau_l \left(1 + \frac{1}{2} v_1^2 + U_1 \right). \quad (\text{B51})$$

As a result,

$$\bar{\delta}_1 = \Delta_1 - \bar{T}_1 - \Delta'_1 \quad (\text{B52})$$

and

$$\bar{\delta}_2 = \Delta_2 + \tau_l \left(\frac{1}{2} v_1^2 + U_1 \right) - \bar{T}_2 - \Delta'_2. \quad (\text{B53})$$

Additional relations between these quantities are obtained by matching the spacetime coordinates of various events that are obtained by two different methods.

5. 2 → 3 parameters

Six independent parameters are obtained from the expressions for \vec{x}_3 . On the one hand, the GS motion implies

$$\begin{aligned} \vec{x}_3 &= \vec{x}_1 + \vec{v}_1(T + P) + \frac{1}{2} \vec{a}_1(T + P)^2 \\ &= \vec{x}_1 + 2\vec{v}_1T + \vec{v}_1\Delta_1 + 2\vec{a}_1T^2. \end{aligned} \quad (\text{B54})$$

On the other hand, an expression for \vec{x}_3 is obtained by following the light pulse B_2 . For the downward motion the closest distance to the centre of the Earth is still $r_3 \equiv r_1$, hence the post-Newtonian correction to the trajectory is

$$\begin{aligned} \vec{\chi}_\downarrow &:= \vec{\chi}_\downarrow(\vec{x}_2, \hat{n}_{23}, P) = 2M\hat{n}_{12} \ln \frac{r_1 - \hat{n}_{12} \cdot \vec{x}_1}{r_2 - \hat{n}_{12} \cdot \vec{x}_2} \\ &\quad - 2 \frac{M\vec{d}_1}{d_1^2} \left(r_1 - r_2 + \frac{\hat{n}_{12} \cdot \vec{x}_2}{r_2} T \right), \end{aligned} \quad (\text{B55})$$

where here and in the following we use the fact that $T = \bar{T} = P = P'$ to leading order. We also rewrite

$$\begin{aligned} \vec{\chi}_\uparrow &:= \vec{\chi}_\uparrow(\vec{x}_1, \hat{n}_{12}, T) = -2M\hat{n}_{12} \ln \frac{r_2 + \hat{n}_{12} \cdot \vec{x}_2}{r_1 + \hat{n}_{12} \cdot \vec{x}_1} \\ &\quad - 2 \frac{M\vec{d}_1}{d_1^2} \left(r_2 - r_1 - \frac{\hat{n}_{12} \cdot \vec{x}_1}{r_1} T \right). \end{aligned} \quad (\text{B56})$$

In the above expressions we use the leading-order identity $\vec{x}_2 = \vec{x}_1 + \hat{n}_{12}T$. Finally, an alternative expression for \vec{x}_3 is

$$\begin{aligned} \vec{x}_3 &= \vec{x}_1 + \hat{n}_{12}T + \hat{n}_{23}P + \vec{\chi}_\uparrow + \vec{\chi}_\downarrow \\ &= \vec{x}_1 - \hat{n}_{12}\Delta_1 + \vec{v}_1T \\ &\quad - \hat{n}_{12}\Delta_2 + \vec{v}_1\Delta_1 + \vec{v}_2T + \vec{\chi}_\uparrow + \vec{\chi}_\downarrow. \end{aligned} \quad (\text{B57})$$

Comparison of Eqs. (B54) and (B57) leads to the identification of the first-order terms as

$$2\vec{v}_1T = \vec{v}_1T - \hat{n}_{12}\Delta_1, \quad (\text{B58})$$

resulting in

$$\Delta_1 = -2\mathfrak{d}_1T, \quad (\text{B59})$$

and

$$\vec{v}_1 = -2\hat{n}_{12}\mathfrak{d}_1 + 2\vec{v}_1. \quad (\text{B60})$$

The second-order equation is

$$\vec{v}_1\Delta_1 + 2\vec{a}_1T^2 = -\hat{n}_{12}\Delta_2 + \vec{v}_1\Delta_1 + \vec{v}_2T + \vec{\chi}_\uparrow + \vec{\chi}_\downarrow, \quad (\text{B61})$$

which results in

$$\Delta_2 = -\mathfrak{d}_1\Delta_1 - 2\mathfrak{a}_1T^2 + \frac{1}{2}\nu_1^2T + \chi_\uparrow + \chi_\downarrow, \quad (\text{B62})$$

where $\chi_{\uparrow,\downarrow} := \hat{n}_{12} \cdot \vec{\chi}_{\uparrow,\downarrow}$ and

$$\vec{v}_2 = (\vec{v}_1\Delta_1 + 2\vec{a}_1T^2 + \hat{n}_{12}\Delta_2 - \vec{v}_1\Delta_1 - \vec{\chi}_\uparrow - \vec{\chi}_\downarrow)/T. \quad (\text{B63})$$

6. $\bar{\mathbf{1}} \rightarrow \bar{\mathbf{2}}$ parameters

At order ϵ^2 the two expressions for the SC position \vec{x}_2 are

$$\begin{aligned}\vec{x}_2 &= \vec{x}_1 + \hat{n}_{12}\bar{T} + \vec{\chi}_\uparrow(\vec{x}_1, \hat{n}_{12}, \bar{T}) \\ &= \vec{x}_1 + \hat{n}_{12}T + \underline{\vec{v}}_1T + \hat{n}_{12}\bar{T}_1 \\ &\quad + \underline{\vec{v}}_2T + \underline{\vec{v}}_1\bar{T}_1 + \hat{n}_{12}\bar{T}_2 + \vec{\chi}_\uparrow(\vec{x}_1, \hat{n}_{12}, T),\end{aligned}\quad (\text{B64})$$

where

$$\vec{x}_1 = \vec{x}_1 + \vec{v}_1(\tau_l + \delta_1) + \frac{1}{2}\vec{a}_1\tau_l^2, \quad (\text{B65})$$

and

$$\begin{aligned}\vec{x}_2 &= \vec{x}_2 + \vec{v}_2(t_2 - t_2) + \frac{1}{2}\vec{a}_2(t_2 - t_2)^2 \\ &= \vec{x}_1 + \hat{n}_{12}T + \vec{\chi}_\uparrow(\vec{x}_1, \hat{n}_{12}, T) + \vec{v}_2(\tau_l + \delta_1 + \bar{T}_1) \\ &\quad + \frac{1}{2}\vec{a}_2\tau_l^2,\end{aligned}\quad (\text{B66})$$

as this is where the SC is at the moment $t_2 = t_1 + \bar{T}$. The first six equations (which contain seven variables) are

$$\vec{v}_1\tau_l + \underline{\vec{v}}_1T + \hat{n}_{12}\bar{T}_1 = \vec{v}_2\tau_l, \quad (\text{B67})$$

at order ϵ and

$$\begin{aligned}\vec{v}_1\delta_1 + \frac{1}{2}\vec{a}_1\tau_l^2 + \underline{\vec{v}}_2T + \underline{\vec{v}}_1\bar{T}_1 + \hat{n}_{12}\bar{T}_2 \\ = \vec{v}_2(\delta_1 + \bar{T}_1) + \frac{1}{2}\vec{a}_2\tau_l^2,\end{aligned}\quad (\text{B68})$$

at order ϵ^2 .

We get from the first-order equations (which are self-contained)

$$\bar{T}_1 = (\mathbf{d}_2 - \mathbf{d}_1)\tau_l \equiv T_1, \quad (\text{B69})$$

$$\underline{\vec{v}}_1 = ((\vec{v}_2 - \vec{v}_1) - \hat{n}_{12}(\mathbf{d}_2 - \mathbf{d}_1))\tau_l/T \equiv \vec{v}_1^*. \quad (\text{B70})$$

The second-order term \bar{T}_2 is given below after we identify $\bar{\delta}_1$.

7. $\bar{\mathbf{1}} \rightarrow \bar{\mathbf{2}} \rightarrow \mathbf{3}^*$ vs $\mathbf{1} \rightarrow \mathbf{2} \rightarrow \mathbf{3} \rightarrow \mathbf{3}^*$ parameters

Since the difference between $\tau_l \equiv \tau_{33^*}^{\text{GS}}$ and t_{33^*} is on the order of ϵ^2 , following the GS leads to

$$\vec{x}_{3^*} = \vec{x}_3 + \vec{v}_3\tau_l + \frac{1}{2}\vec{a}_3\tau_l^2, \quad (\text{B71})$$

where the second-order expression for \vec{v}_3 is

$$\vec{v}_3 = \vec{v}_1 + 2\vec{a}_1T. \quad (\text{B72})$$

Since $\tau_l/T \sim \mu \sim 10^{-3}$, we discard the term in the correction of the velocity and since $\vec{a}_3 = \vec{a}_1 + \mathcal{O}(\epsilon^3)$, we set $\vec{a}_3 = \vec{a}_1$. Hence,

$$\begin{aligned}\vec{x}_{3^*} &= \vec{x}_1 - \hat{n}_{12}\Delta_1 + \vec{v}_1T - \hat{n}_{12}\Delta_2 + \vec{v}_1\Delta_1 + \vec{v}_2T \\ &\quad + \vec{\chi}_\uparrow + \vec{\chi}_\downarrow + \vec{v}_1\tau_l + \vec{a}_1\tau_l\left(2T + \frac{1}{2}\tau_l\right).\end{aligned}\quad (\text{B73})$$

This expression should be matched with the result of tracing B_1 from $\bar{\mathbf{2}}$ to $\mathbf{3}^*$,

$$\begin{aligned}\vec{x}_{3^*} &= \vec{x}_2 + \hat{n}_{23^*}P' + \vec{\chi}_\downarrow(\vec{x}_2, \hat{n}_{23^*}, P') \\ &= \vec{x}_2 - \hat{n}_{12}T - \hat{n}_{12}\Delta'_1 + \vec{v}'_1T \\ &\quad - \hat{n}_{12}\Delta'_2 + \vec{v}'_1\Delta'_1 + \vec{v}'_2T + \vec{\chi}_\downarrow(\vec{x}_2, \hat{n}_{23^*}, P),\end{aligned}\quad (\text{B74})$$

that, by using Eq. (B66), becomes

$$\begin{aligned}\vec{x}_{3^*} &= \vec{x}_1 + \vec{\chi}_\uparrow + \vec{v}_2(\tau_l + \delta_1 + \bar{T}_1) + \frac{1}{2}\vec{a}_2\tau_l^2 \\ &\quad - \hat{n}_{12}\Delta'_1 + \vec{v}'_1T - \hat{n}_{12}\Delta'_2 + \vec{v}'_1\Delta'_1 + \vec{v}'_2T + \vec{\chi}_\downarrow.\end{aligned}\quad (\text{B75})$$

From the coincidence of the beams at \vec{x}_{3^*} we obtain a further six equations,

$$-\hat{n}_{12}\Delta_1 + \vec{v}_1T + \vec{v}_1\tau_l = -\hat{n}_{12}\Delta'_1 + \vec{v}'_1T + \vec{v}_2\tau_l, \quad (\text{B76})$$

at order ϵ , and

$$\begin{aligned}-\hat{n}_{12}\Delta_2 + \vec{v}_1\Delta_1 + \vec{v}_2T + \vec{a}_1\tau_l\left(2T + \frac{1}{2}\tau_l\right) \\ = -\hat{n}_{12}\Delta'_2 + \vec{v}'_1\Delta'_1 + \vec{v}'_2T + \vec{v}_2(\delta_1 + \bar{T}_1) + \frac{1}{2}\vec{a}_2\tau_l^2,\end{aligned}\quad (\text{B77})$$

at order ϵ^2 . From Eq. (B76) we get

$$\Delta'_1 = \Delta_1 + (\mathbf{d}_2 - \mathbf{d}_1)\tau_l = -2\mathbf{d}_1T + (\mathbf{d}_2 - \mathbf{d}_1)\tau_l \quad (\text{B78})$$

[note that $(\Delta' - \Delta)/T \sim \mathcal{O}(\epsilon\mu)$] and

$$\begin{aligned}\vec{v}'_1 &= \vec{v}_1 + (\hat{n}_{12}(\Delta'_1 - \Delta_1) + (\vec{v}_1 - \vec{v}_2)\tau_l)/T \\ &= \vec{v}_1 + (\hat{n}_{12}(\mathbf{d}_1 - \mathbf{d}_2) + \vec{v}_1 - \vec{v}_2)\tau_l/T \\ &= \vec{v}_1 - \vec{v}_1^*,\end{aligned}\quad (\text{B79})$$

and calculation of the first-order terms is completed by

$$\bar{\delta}_1 = \Delta_1 - \Delta'_1 - \bar{T}_1 = -2(\mathbf{d}_2 - \mathbf{d}_1)\tau_l \equiv 2\delta_1 = -2T_1. \quad (\text{B80})$$

This is the basis for the Doppler cancellation scheme.

Now we combine this result with Eq. (B68) to obtain

$$\begin{aligned}\bar{T}_2 &= -2\mathbf{d}_1\delta_1 - \frac{1}{2}\mathbf{a}_1\tau_l^2 + \frac{1}{2}\nu_1^2 T + \mathbf{d}_2\delta_1 + \frac{1}{2}\mathbf{a}_2\tau_l^2 \\ &= (\mathbf{d}_2 - \mathbf{d}_1)(2\mathbf{d}_1 - \mathbf{d}_2)\tau_l + \frac{1}{2}(\mathbf{a}_2 - \mathbf{a}_1)\tau_l^2 \\ &\quad + \frac{1}{2}((\vec{v}_2 - \vec{v}_1)^2 - (\mathbf{d}_2 - \mathbf{d}_1)^2)\tau_l^2/T.\end{aligned}\quad (\text{B81})$$

From Eq. (B77) we get

$$\begin{aligned}-\Delta_2 + \frac{1}{2}\nu_1^2 T + \mathbf{a}_1\tau_l\left(2T + \frac{1}{2}\tau_l\right) \\ = -\Delta'_2 + \frac{1}{2}\nu_1^2 T + \mathbf{d}_2(2\delta_1 + T_1) + \frac{1}{2}\mathbf{a}_2\tau_l^2.\end{aligned}\quad (\text{B82})$$

Using Eq. (B79) we obtain

$$\nu_1^2 = \nu_1^2 + 2\vec{v}_1 \cdot (\vec{v}_1 - \vec{v}_2)\tau_l/T + \mathcal{O}(\epsilon^2\mu^2).\quad (\text{B83})$$

Applying Eqs. (B30) and (B80) as $2\delta_1 + T_1 = \delta_1 = (\mathbf{d}_2 - \mathbf{d}_1)\tau_l$ to the above result leads to

$$\Delta'_2 = \Delta_2 - 2\mathbf{a}_1\tau_l T + \vec{v}_1 \cdot (\vec{v}_1 - \vec{v}_2)\tau_l + \mathbf{d}_2\delta_1 + \frac{1}{2}(\mathbf{a}_2 - \mathbf{a}_1)\tau_l^2.\quad (\text{B84})$$

Using Eq. (B60) this expression reduces to

$$\begin{aligned}\Delta_2 - \Delta'_2 &= 2\mathbf{a}_1\tau_l T - \vec{v}_1 \cdot (\vec{v}_1 - \vec{v}_2)\tau_l \\ &\quad + \mathbf{d}_2(\mathbf{d}_2 - \mathbf{d}_1)\tau_l - \frac{1}{2}(\mathbf{a}_2 - \mathbf{a}_1)\tau_l^2 \\ &= 2\mathbf{a}_1\tau_l T - (2\mathbf{d}_1 - \mathbf{d}_2)(\mathbf{d}_2 - \mathbf{d}_1)\tau_l \\ &\quad - 2\vec{v}_1 \cdot (\vec{v}_1 - \vec{v}_2)\tau_l - \frac{1}{2}(\mathbf{a}_2 - \mathbf{a}_1)\tau_l^2.\end{aligned}\quad (\text{B85})$$

8. Phase difference at the GS

By noting that

$$\begin{aligned}\tau_{1\bar{1}}^{\text{GS}} &= t_{1\bar{1}}\left(1 - \frac{1}{2}v_1^2 - U_1\right) \\ &= (\tau_l - 2T_1 + \bar{\delta}_2)\left(1 - \frac{1}{2}v_1^2 - U_1\right) \\ &= \tau_l - 2T_1 + \left(\bar{\delta}_2 - \tau_l\left(\frac{1}{2}v_1^2 + U_1\right)\right),\end{aligned}\quad (\text{B86})$$

we can write

$$\begin{aligned}\tau_{1\bar{1}}^{\text{GS}} - \tau_l &= -2T_1 + \left(\bar{\delta}_2 - \tau_l\left(\frac{1}{2}v_1^2 + U_1\right)\right) \\ &=: -2T_1 + \Delta^{(2)},\end{aligned}\quad (\text{B87})$$

where $\Delta^{(2)}$ is defined according to Eq. (B53) as

$$\begin{aligned}\Delta^{(2)} &:= \Delta_2 - \Delta'_2 - \bar{T}_2 \\ &= 2\mathbf{a}_1\tau_l T - 2(2\mathbf{d}_1 - \mathbf{d}_2)(\mathbf{d}_2 - \mathbf{d}_1)\tau_l - 2\vec{v}_1 \cdot (\vec{v}_1 - \vec{v}_2)\tau_l \\ &\quad - (\mathbf{a}_2 - \mathbf{a}_1)\tau_l^2 - \frac{1}{2}((\vec{v}_2 - \vec{v}_1)^2 - (\mathbf{d}_2 - \mathbf{d}_1)^2)\tau_l^2/T.\end{aligned}\quad (\text{B88})$$

In the end, the phase difference at the GS results

$$\varphi_{\text{GS}} = \omega_0(\tau_{1\bar{1}}^{\text{GS}} - \tau_l) = -2\omega_0 T_1 + \varphi_{\text{GS}}^{(2)}\quad (\text{B89})$$

with

$$\varphi_{\text{GS}}^{(2)} = \omega_0\Delta^{(2)}.\quad (\text{B90})$$

9. The signal

Having the explicit expressions for φ_{SC} and φ_{GS} up to the second order, we obtain

$$\begin{aligned}S &= \varphi_{\text{SC}} - \frac{1}{2}\varphi_{\text{GS}} = \varphi_{\text{SC}}^{(2)} - \frac{1}{2}\varphi_{\text{GS}}^{(2)} \\ &= \omega_0\left(\tau_l\left[\frac{1}{2}(v_2^2 - v_1^2) + U_2 - U_1\right] - T_2 - \frac{1}{2}\Delta^{(2)}\right)\end{aligned}\quad (\text{B91})$$

that explicitly reads

$$\begin{aligned}\frac{S}{\omega_0\tau_l} &= U_2 - U_1 + \frac{1}{2}(v_2^2 - v_1^2) \\ &\quad + \vec{v}_1 \cdot (\vec{v}_1 - \vec{v}_2) - (\mathbf{d}_2 - \mathbf{d}_1)^2 - \mathbf{a}_1 T \\ &\quad - \frac{\tau_l}{4T}((\vec{v}_2 - \vec{v}_1)^2 - (\mathbf{d}_2 - \mathbf{d}_1)^2),\end{aligned}\quad (\text{B92})$$

and leads to Eq. (5).

APPENDIX C: UNEQUAL DELAY LINES

As discussed above, it is impossible for two delay lines to be perfectly identical. We characterize the difference in the proper propagation times as

$$\tau_l^{\text{GS}} = \tau_l, \quad \tau_l^{\text{SC}} = \tau_l + \Delta\tau_l := \tau_l(1 + \delta_l),\quad (\text{C1})$$

and we assume that the relative difference of the delay lines is at most of the order

$$\delta_l = \frac{\tau_l^{\text{SC}} - \tau_l^{\text{GS}}}{\tau_l^{\text{GS}}} = \frac{\Delta\tau_l}{\tau_l} \lesssim 10^{-6} \sim \epsilon^{6/5}.\quad (\text{C2})$$

The analysis of the two-way trip (Appendix B 3) does not change. On the other hand, for the one-way trip

(Appendix B 2) we now have instead of Eq. (B18) the following relation

$$\tau_l(1 + \delta_l) \equiv \tau_{22^*}^{\text{SC}} = t_{22^*} \left(1 - \frac{1}{2}v_2^2 - U_2\right), \quad (\text{C3})$$

so that Eq. (B19) becomes

$$t_{22^*} = \tau_l \left(1 + \delta_l + \frac{1}{2}v_2^2 + U_2\right). \quad (\text{C4})$$

The rest of the calculations proceed as before, resulting in the departure coordinate time (GRF) of the beam A_1 . Using the results for T_1 and T_2 we get

$$t_{11^*} = \tau_l \left(1 + \delta_l + \frac{1}{2}v_2^2 + U_2\right) - T_1 - T_2. \quad (\text{C5})$$

Accordingly,

$$\tau_{11^*}^{\text{SC}} - \tau_l = -T_1 + \tau_l \left(\delta_l + \frac{1}{2}(v_2^2 - v_1^2) + U_2 - U_1\right) - T_2, \quad (\text{C6})$$

where the term T_1 is responsible for the first-order Doppler effect in the phase difference at the SC

$$\varphi_{\text{SC}} = \omega_0(\tau_{11^*}^{\text{SC}} - \tau_l) = -\omega_0 T_1 + \omega_0 \tau_l \delta_l + \varphi_{\text{SC}}^{(2)}, \quad (\text{C7})$$

$\omega_0 \tau_l \delta_l$ a constant offset, and the higher-order corrections related to the mismatch of the delay times are at least of the order $\mathcal{O}(\epsilon^3)$.

Effects of the constant delay line mismatch $\Delta l = l \delta_l$ can be removed by data processing. However, a random time-varying mismatch can wash out the imprints of the gravitational redshift (and the second-order effects in general). The most immediate source of randomness are the temperature fluctuations that give

$$\Delta \delta_l \approx \kappa \Delta \mathbb{T}, \quad (\text{C8})$$

where κ is the thermal expansion coefficient and $\Delta \mathbb{T}$ is the onboard temperature fluctuation during one passage of the satellite. Given the results of Sec. IV, having $\Delta \delta_l \sim 10^{-11}$ allows for the identification of second-order effects, and $\Delta \delta_l \sim 10^{-13} - 10^{-15}$ allows for precision measurements of the gravitational redshift. If $\kappa \sim 10^{-7} - 10^{-9} \text{ K}^{-1}$ and the maximal temperature variation $\Delta \mathbb{T} \sim 10^{-5} \text{ K}$ as in the desiderata list of the ORTIS mission [65], then not only identification of ΔU , but also putting the EM-based bounds on α is possible. Current results from the pathfinder missions [66,67] reliably set $\Delta \mathbb{T} \lesssim 10^{-3}$, bringing an all-optical measurement of the gravitational redshift into the realm of possibility.

APPENDIX D: INTERFERENCE VISIBILITY

Besides the spatial overlap of the interfering beams (that is granted by the use of single-mode fibers at the two terminals), the different arrival times at the detector can cause a decrease in the interferometric visibility \mathcal{V} , limiting the precision of phase estimation to $\delta \varphi_{gr} \approx 1/(\mathcal{V}\sqrt{N})$, where N is the number of detected photons. Since we are dealing with optical pulses whose line width is much smaller than the central frequency, it is possible to perform all calculations in the monochromatic approximation used in Sec. III and evaluate the visibility by looking at the overlap between the backpropagated pulses at the two different starting points (in the GS reference frame).

Following the conventions of [16], we define the envelope function of a Gaussian pulse centered in t_A as

$$\mathcal{A}_{t_A}(t) = \sqrt{\frac{1}{\pi\tau_c^2}} \exp\left[-\frac{(t-t_A)^2}{2\tau_c^2}\right], \quad (\text{D1})$$

where τ_c is the coherence time of the pulse. The overlap between two pulses centered at t_A and t_B , respectively, is given by the integral

$$\begin{aligned} \mathcal{V} &= \sqrt{\frac{1}{\pi\tau_c^2}} \int dt \exp\left[-\frac{(t-t_A)^2}{2\tau_c^2}\right] \exp\left[-\frac{(t-t_B)^2}{2\tau_c^2}\right] \\ &= \exp\left[-\frac{(t_A-t_B)^2}{4\tau_c^2}\right]. \end{aligned} \quad (\text{D2})$$

From this formula and using the conventions of Sec. III, it is possible to calculate the visibility in the one-way and in the two-way configuration, as

$$\mathcal{V}_{\text{one-way}} = \exp\left[-\frac{(\tau_{11^*}^{\text{GS}} - \tau_l)^2}{4\tau_c^2}\right], \quad (\text{D3})$$

$$\mathcal{V}_{\text{two-way}} = \exp\left[-\frac{(\tau_{11}^{\text{GS}} - \tau_l)^2}{4\tau_c^2}\right]. \quad (\text{D4})$$

By inserting, respectively, Eqs. (B34) and (B86) in the above equations, we obtain at leading order

$$\mathcal{V}_{\text{one-way}} \approx \exp\left[-\frac{T_1^2}{4\tau_c^2}\right] = \exp\left[-\frac{(\mathbf{d}_2 - \mathbf{d}_1)^2 \tau_l^2}{4\tau_c^2}\right], \quad (\text{D5})$$

$$\mathcal{V}_{\text{two-way}} \approx \exp\left[-\frac{T_1^2}{\tau_c^2}\right] = \exp\left[-\frac{(\mathbf{d}_2 - \mathbf{d}_1)^2 \tau_l^2}{\tau_c^2}\right]. \quad (\text{D6})$$

As evident from the previous equations, the visibility depends on $(\tau_l/\tau_c)^2$. We have verified that, given an imbalance $\tau_l = 6 \mu\text{s}$ and a coherence time of $\tau_c = 10 \text{ ns}$, the visibility is higher than 99% for all studied trajectories and its effect can be neglected.

- [1] C. W. Misner, K. S. Thorne, and J. A. Wheeler, *Gravitation* (Freeman, San Francisco, 1973).
- [2] C. M. Will, *Theory and Experiment in Gravitational Physics* (Cambridge University Press, Cambridge, England, 2018), 2nd ed.
- [3] E. Poisson and C. M. Will, *Gravity: Newtonian, Post-Newtonian, Relativistic* (Cambridge University Press, Cambridge, England, 2014).
- [4] M. Born and E. Wolf, *Principles of Optics* (Cambridge University Press, Cambridge, England, 1999), 7th ed.
- [5] L. Mandel and E. Wolf, *Optical Coherence and Quantum Optics* (Cambridge University Press, Cambridge, England, 1995).
- [6] D. R. Terno, *Phys. Rev. A* **89**, 042111 (2014).
- [7] R. Colella, A. W. Overhauser, and S. Werner, *Phys. Rev. Lett.* **34**, 1472 (1975).
- [8] M. Zych, F. Costa, I. Pikovski, and Č. Brukner, *Nat. Commun.* **2**, 505 (2011).
- [9] D. Rideout *et al.*, *Classical Quantum Gravity* **29**, 224011 (2012).
- [10] T. Jennewein *et al.*, in *Proceedings SPIE 8997, Advances in Photonics of Quantum Computing, Memory, and Communication VII: 89970A* (2014), 10.1117/12.2041693.
- [11] J. Brendel, N. Gisin, W. Tittel, and H. Zbinden, *Phys. Rev. Lett.* **82**, 2594 (1999).
- [12] D. R. Terno, G. Vallone, F. Vedovato, and P. Villoresi, *Phys. Rev. D* **101**, 104052 (2020).
- [13] The linear approximation of the difference of the gravitational potential gh , used on the right-hand side of Eq. (1), would give $\Delta U \approx -1.6 \times 10^{-10}$.
- [14] R. Demkowicz-Dobrzański, M. Jarzyna, and J. Kołodyński, *Prog. Opt.* **60**, 345 (2015).
- [15] A. Brodutch, A. Gilchrist, T. Guff, A. R. H. Smith, and D. R. Terno, *Phys. Rev. D* **91**, 064041 (2015).
- [16] G. Vallone, D. Dequal, M. Tomasin, F. Vedovato, M. Schiavon, V. Luceri, G. Bianco, and P. Villoresi, *Phys. Rev. Lett.* **116**, 253601 (2016).
- [17] F. Vedovato *et al.*, *Sci. Adv.* **3**, e1701180 (2017).
- [18] M. Zych, F. Costa, I. Pikovski, T. C. Ralph, and Č. Brukner, *Classical Quantum Gravity* **29**, 224010 (2012).
- [19] J. Yin *et al.*, *Science* **356**, 1140 (2017).
- [20] J. G. Ren *et al.*, *Nature (London)* **549**, 70 (2017).
- [21] K. Danzmann (The LISA Study Team), *Classical Quantum Gravity* **13**, A247 (1996).
- [22] S. K. Liao *et al.*, *Nature (London)* **549**, 43 (2017).
- [23] D. K. L. Oi *et al.*, *Eur. Phys. J. Quantum Technol.* **4**, 6 (2017).
- [24] R. Bedington, J. M. Arrazola, and A. Ling, *npj Quantum Inf.* **3**, 30 (2017).
- [25] C. Agnesi *et al.*, *Phil. Trans. R. Soc. A* **376**, 20170461 (2018).
- [26] I. Khan, B. Heim, A. Neuzner, and C. Marquardt, *Opt. Photonics News* **29**, 26 (2018).
- [27] S. K. Liao *et al.*, *Phys. Rev. Lett.* **120**, 030501 (2018).
- [28] I. Ciufolini and J. A. Wheeler, *Gravitation and Inertia* (Princeton University Press, Princeton, NJ, 1995).
- [29] C. M. Will, *Living Rev. Relativity* **17**, 4 (2014).
- [30] P. A. M. Dirac, *Nature (London)* **139**, 323 (1937).
- [31] J.-P. Uzan, *Living Rev. Relativity* **14**, 2 (2011).
- [32] R. Lange, N. Huntemann, J. M. Rahm, C. Sanner, H. Shao, B. Lipphardt, Chr. Tamm, S. Weyers, and E. Peik, *Phys. Rev. Lett.* **126**, 011102 (2021).
- [33] A. Einstein, *Ann. Phys. (N.Y.)* **35**, 898 (1911).
- [34] D. Colladay and V. A. Kostelecký, *Phys. Rev. D* **58**, 116002 (1998).
- [35] V. A. Kostelecký and N. Russell, *Rev. Mod. Phys.* **83**, 11 (2011).
- [36] S. Liberati, *Classical Quantum Gravity* **30**, 133001 (2013).
- [37] M. A. Hohensee, S. Chu, A. Peters, and H. Müller, *Phys. Rev. Lett.* **106**, 151102 (2011).
- [38] J. C. LoPresto, C. Schrader, and A. K. Pierce, *Astrophys. J.* **376**, 757 (1991).
- [39] R. V. Pound and G. A. Rebka, Jr., *Phys. Rev. Lett.* **4**, 337 (1960).
- [40] R. F. C. Vessot *et al.*, *Phys. Rev. Lett.* **45**, 2081 (1980).
- [41] F. Meynadier, P. Delva, C. le Poncin-Lafitte, C. Guerlin, and P. Wolf, *Classical Quantum Gravity* **35**, 035018 (2018).
- [42] N. Ashby, T. E. Parker, and B. R. Patla, *Nat. Phys.* **14**, 822 (2018).
- [43] P. Delva *et al.*, *Phys. Rev. Lett.* **121**, 231101 (2018).
- [44] S. Herrmann *et al.*, *Phys. Rev. Lett.* **121**, 231102 (2018).
- [45] T. Bothwell, C. J. Kennedy, A. Aeppli, D. Kedar, J. M. Robinson, E. Oelker, A. Staron, and J. Ye, *Nature (London)* **602**, 420 (2022).
- [46] K. Van Tilburg, N. Leefer, L. Bougas, and D. Budke, *Phys. Rev. Lett.* **115**, 011802 (2015).
- [47] H. Takenaka, M. Toyoshima, and Y. Takayama, *Opt. Express* **20**, 15301 (2012).
- [48] M. W. Wright, J. F. Morris, J. M. Kovalik, K. S. Andrews, M. J. Abrahamson, and A. Biswas, *Opt. Express* **23**, 33705 (2015).
- [49] M. Tinto and S. V. Dhurandhar, *Living Rev. Relativity* **17**, 6 (2014).
- [50] R. F. C. Vessot and M. W. Levine, NASA Technical Report No. NASA-CR-161409, 1979 (unpublished).
- [51] M. R. Pearlman, J. J. Degnan, and J. M. Bosworth, *Adv. Space Res.* **30**, 135 (2002).
- [52] https://ilrs.cddis.eosdis.nasa.gov/data_and_products/formats/cpf.html.
- [53] https://ilrs.cddis.eosdis.nasa.gov/network/stations/active/MATM_general.html.
- [54] G. Vallone, D. Bacco, D. Dequal, S. Gaiarin, V. Luceri, G. Bianco, and P. Villoresi, *Phys. Rev. Lett.* **115**, 040502 (2015).
- [55] D. Dequal, G. Vallone, D. Bacco, S. Gaiarin, V. Luceri, G. Bianco, and P. Villoresi, *Phys. Rev. A* **93**, 010301(R) (2016).
- [56] L. Calderaro, C. Agnesi, D. Dequal, F. Vedovato, M. Schiavon, A. Santamato, V. Luceri, G. Bianco, G. Vallone, and P. Villoresi, *Quantum Sci. Technol.* **4**, 015012 (2019).
- [57] C. Agnesi, L. Calderaro, D. Dequal, F. Vedovato, M. Schiavon, A. Santamato, V. Luceri, G. Bianco, G. Vallone, and P. Villoresi, *J. Opt. Soc. Am. B* **36**, B59 (2019).
- [58] <https://nssdc.gsfc.nasa.gov/nmc/spacecraft/display.action?id=1993-079A>.
- [59] <https://www.orekit.org/>.
- [60] J. W. Goodman, *Statistical Optics* (John Wiley, Hoboken, 2015), 2nd ed.
- [61] G. B. Xavier and J. P. von der Weid, *Opt. Lett.* **36**, 1764 (2011).

- [62] A. Fix, C. Büdenbender, M. Wirth, M. Quatrevalet, A. Amediak, C. Kiemle, and G. Ehret, in *Proceedings SPIE 8182, Lidar Technologies, Techniques, and Measurements for Atmospheric Remote Sensing VII, 818206* (2011), 10.1117/12.898412.
- [63] F. Elsen *et al.*, *Opt. Eng.* **57**, 021205 (2017).
- [64] C. Robert, J.-M. Conan, and P. Wolf, *Phys. Rev. A* **93**, 033860 (2016).
- [65] C. Lämmerzahl, H. Dittus, A. Peters, and S. Schiller, *Classical Quantum Gravity* **18**, 2499 (2001).
- [66] M. Armano *et al.*, *Mon. Not. R. Astron. Soc.* **486**, 3368 (2019).
- [67] X. Zhang, H. Liang, H. Tan, J. Feng, and H. Li (The Taiji Scientific Collaboration), *Int. J. Mod. Phys. A* **36**, 2140022 (2021).